Type-I intermittency for the Hénon-map family

Harvey Kaplan
Department of Physics, Syracuse University, Syracuse, New York 13244-1130
(Received 4 January 1993)

Type-I intermittency was defined as the precursor quasiregular behavior to every tangent bifurcation for the one-dimensional (1D) quadratic-map family. We have extended the definition to the two-dimensional Hénon-map family with the following results. The gradual increase of bistability and multistability that accompanies the reduction of dissipation from the 1D limit carries with it the eventual decrease and disappearance of the intermittency associated with the occurrence of each stable periodic orbit. Numerically we observe qualitative changes in the invariant orbit density and the Lyapunov exponent in the transition region, the latter showing a discontinuous, or first-order, rather than the usual continuous phase transition. A hysteretic response of the dynamics to slow parameter change, which usually accompanies a first-order transition, is also noted. The changes associated with various periodic orbits, which are tabulated, show both similarities and differences. A considerable understanding of these phenomena is achieved by an in-depth study of the topology of, and dynamics in, the phase plane of the Hénon system. Heuristic pictures are developed for some surprising bifurcation structures.

PACS number(s): 05.45.+b

I. INTRODUCTION

Type-I intermittency was defined by Pomeau and Manneville for the logistic-map family, $y_{n+1}=\mu-y_n^2$, as the quasiregular period-n behavior that precedes the tangent bifurcation of period n that ushers in each period-n parameter window of stability [1]. Here a family member is defined by a value of μ; *some* unique attractor exists for $-0.25\le\mu<2.0$. In a recent publication [2], I described the changes in type-I intermittency that occur for constant-J subfamilies, with $J>0$, of the Hénon-map family

$$x_{n+1}=y_n,\quad y_{n+1}=-Jx_n+\mu-y_n^2\ ,$$

preceding the period-3 saddle-node bifurcation. Here, the subfamily defined by $J=0$ is identical to the logistic-map family mentioned above. The $J>0$ subfamilies are referred to as orientation preserving, and arise from a continuous-flow system as shown by Schuster [3]. The necessity for such changes is clear. For $J=0$, Singer's theorem establishes the existence of one attractor for each parameter value, and thus the entire trapping region is one basin of attraction (BA). The structure of the parameter window of stability following each tangent bifurcation, notably its end at a Misiurewicz point [4], makes it clear that some form of aperiodic behavior is disrupted whenever a tangent bifurcation occurs. Works by Hénon [5], by Holmes and Whitley [6], and by El-Hamouli and Mira [7] show that, when J increases above zero, multistability becomes ever more prevalent, so that aperiodic behavior in one BA is not necessarily interrupted when a saddle-node bifurcation occurs. In the area-preserving limit, $J=1$, an infinite number of elliptic basins (the area-preserving analogs of basins of attraction) exist for most values of μ for which a trapping region exists. It was not clear for what $J>0$ subfamily changes first occur, and exactly what these changes would be. As described in Ref. [2], an increase in J above $J=0$ results in qualitative changes in period-3 intermittency at two values of J, namely $J^*(3)$, and $J'(3)$. When $J<J^*(3)$, intermittency occurs just preceding the period-3 saddle-node bifurcation at $\mu=s_3(J)$ exactly as at $J=0$, and no bistability of the period-1 and period-3 basins of attraction (BA's) is possible. When $J'(3)>J>J^*(3)$, bistability of period-3 and period-1 BA's is possible, and is accompanied by hysteresis, with variation of μ as described in detail below. In this case, period-3 intermittency occurs after the period-3 BA is created, and turns into regular behavior associated with a period-3 window of stability before the bursts of regular period-3 behavior become very long. When $J>J'(3)$, the bistability is in some sense "complete." Period-3 intermittency and period-1–period-3 hysteresis can no longer accompany the existence of the period-3 BA; one may say that the onset of the period-3 BA has no 3-like precursor. It is of some importance that the numerical values $J^*(3)=0.001\,15$, and $J'(3)=0.018\,13$ are both very small, calling into question the use of the logistic model of intermittency in comparisons with laboratory experiments.

In addition to a somewhat detailed account of period-3 intermittency, Ref. [2] also gave the single number $J^*(n,k)$, corresponding to $J^*(3)$, associated with a qualitative change in intermittent behavior, for a few other periodic orbits, where (n,k) denotes the kth stable periodic orbit occurring at $J=0$ in order of increasing μ. (This number will be defined below.) The purpose of the present paper is to flesh out the reasoning and computational methods used in the period-3 case, and to extend the detailed results to a number of higher-period cases. From a practical point of view (defined as affecting measurement on real physical systems) it is not necessary to discuss very high periods, because parameter windows of periodic stability decrease rapidly with increasing period, and parameter intervals of intermittent behavior always

 ©1993 The American Physical Society

are narrower than the parameter windows of stability with which they are associated. This remark presupposes that the Hénon map, as a low-dimensional map, is most frequently an abstraction of an important low-dimensional subsystem of a large system, and that the remainder of the large system, although not requiring as detailed treatment as the important part modeled by the Hénon map, can be considered to create some noise that has been shown to wash out detail in low-dimensional-map properties.

The complications of the structure seen in a parameter-plane bifurcation diagram of the Hénon-map family cause the intermittency structure in parameter space for many periods higher than 3 to be more complicated then that for period 3. These complications are caused by the intricate crossings of important bifurcation lines in the (J,μ) parameter plane. In particular, the crossing of a potentially intermittent saddle-node line with various members of the period-1 homoclinic fan, which, with increasing J, grows out of the immensely degenerate first Misiurewicz point [4] which occurs at $J=0.0,\mu=2.0$, are noteworthy.

In Sec. II, we discuss some features of the $J=0$ limit which serve as both computational and interpretive guides for the trickier $J>0$ calculations. This discussion is couched almost entirely in terms of the period-3 case, but also applies to most other periodic windows. In Sec. III, we discuss some general features of maps with $J>0$. In Sec. IV, we discuss the period-3 case in detail. In Sec. V, we indicate the complications occurring for many other periodic orbits and estimate how high the period and orbit type need to be followed practically in order to include intermittency that is likely to be observed. Extensions to more complex maps are hinted at in the conclusions in Sec. VI.

II. THE CASE OF $J=0$

The standard features of intermittency for the $J=0$ Hénon subfamily are as follows (couched in the language of the period-3 example).

(1) A time trace of an orbit for a value of μ approaching its period-3 saddle-node value, s_3 from below, shows alternating bursts of period-3 and chaotic behaviors; the period-3 bursts fill an ever larger portion of the time trace as ϵ $(\equiv s_3-\mu)$ decreases toward zero. The average length of period-3 bursts varies as $\epsilon^{-1/2}$.

(2) Concomitantly, the Lyapunov exponent λ varies as $\epsilon^{1/2}$. Note that there is only one Lyapunov exponent because of Singer's theorem.

(3) The invariant-orbit density plotted as a function of the physical coordinate, y, macroscopically shows a symmetric resonance peak centered near each incipient period-3 orbit point. Each peak, when looked at more closely, shows a detailed structure having many primary square-root singularities, with further structure between these. The number of these singularities increases as ϵ decreases, even though the widths of the peaks decrease. This phenomenon was first noted by Fraser and Kapral [8]. The peak structure is calculated by following a long orbit, typically 10^6 iterates (after eliminating early transient behavior) and ordering the points in a histogram with 2400 boxes covering the y range of the peak. A value of μ is used that is very near to the intermittent limit.

(4) A simple understanding of all of the above rests in an analysis of a plot of y_{n+3} as a function of y_n, as shown in Fig. 1. The inset shows the detailed behavior near an orbit point, immediately indicating the reason for alternating bursts of regular and irregular behavior. The narrowness of the channel in the inset is a hint at the height and structure of the resonance peaks in the invariant-orbit density. Fraser and Kapral point out that the square-root singularities are images of the nearby point of zero slope of $y_{n+3}(y_n)$, a so-called *critical point.* Even the rough structure of the orbit density peaks (to be shown below as part of Sec. IV) can be attributed to the critical points, in the form of approximate returns of square-root singularities after chaotic excursions [9]. This structure occurs, for small ϵ, because the shortness of the attendent chaotic bursts allows a primary square-root singularity to return to the regular region without having been entirely attenuated to background. Of course, each return is at a random point within a peak because, despite its peak-dominated invariant-orbit density, the attractor in the intermittent region is a strange attractor (SA), for which no orbit point ever repeats itself. We also note that the reinjection density from the bursts of chaotic motion is uniform over the region of each peak, an occurrence which is absent in some other intermittency scenarios [10].

There remains a point of interest concerning one-dimensional (1D) intermittency, which will be helpful when we leave $J=0$. It is easily determined that intermittency, although striking when it occurs, is less likely to be seen than the window of stability that it precedes because its parameter window of occurrence is in each case smaller than that of the stability window. In order to study this point in detail, we note that regular bursts having a preassigned number of iterates are unlikely to occur until a value of μ below s_3 at which there is a stability window of a periodic orbit which mimics period-3 behavior for the chosen number of iterates. We will refer to such orbits as 3-*mimics.* The reason for the impor-

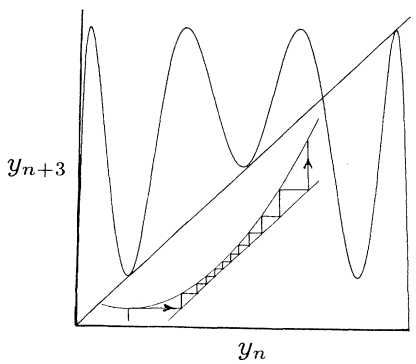

FIG. 1. y_{n+3} (y_n) in the trapping region of the logistic map for μ at an intermittent parameter value preceding the tangent bifurcation to period-3 stability. Inset: The narrow channel giving rise to regular period-3 bursts.

tance of 3-mimics, despite their narrow μ-stability ranges, is that in these windows they replace the regular part of the intermittent orbit, while the chaotic part vanishes.

To elaborate, we first investigate the symbolic dynamics of 3-mimics. For this purpose we use an adaptation of the recursive algorithm of Metropolis, Stein, and Stein (MSS) [11], which finds the order in which the stable periodic orbits occur, complete up to period n, as the parameter μ of a one-hump map increases. The recursion is on the period n, and they dubbed the complete set of such orbits the U sequence. For the logistic family, no finite periodic orbits exist as attractors other than the U sequence. In the MSS topological method, an orbit point is only identified as to whether it lies to the left (L) or to the right (R) of the map maximum, an orbit than consisting of a string of R's and L's called its *symbolic dynamics.* This dynamics is rooted in the topological importance of the map maximum, or *critical point.* MSS realized that the key to identifying the μ order of *stable periodic orbits* consists in a particular comparison of selected time-reversed periodic orbits, or what they called *legal inverse paths* (LIP)'s. For a given logistic map most points do not have unique inverses, there being either zero or two preimages of almost any orbit point. In particular, for $\mu=2.0$, the parameter value for which the map fills its square of definition in the (y_n,y_{n+1}) plane, further identified as the onset of complete chaos, every point (except the two fixed points) has two preimages, so that n inverse iterations produce 2^n preimages of a given point, and therefore 2^n inverse paths of length n. A further ingredient is the occurrence of at least one periodic-orbit point, in a stable periodic orbit of period n, whose image is very near to the critical point, this being necessary in order that the (common) slope at all stable periodic-orbit points have a magnitude less than one. The direct procedure for finding LIP's for period-n stable periodic orbits is to take the map for $\mu=2$, and follow all possible inverse orbits of the *critical point* for $n-1$ steps, creating a set of candidates for, by definition, *superstable* orbits. A LIP for a stable periodic orbit of period n consists of a set of $(n-1)$ R's and L's read and traversed from right to left, such that its last symbol (i.e., furthest to the left) is an R, and the orbit point that it corresponds to is the furthest to the right of all $(n-1)$ orbit points in the LIP. This allows the last point in any LIP to be joined to the central point, if μ is decreased sufficiently from 2.0, thus forming a stable periodic orbit. The required decrease is smaller the further to the right is the last LIP point. The symbol for the central point is not included because during the parameter range of stability of every periodic orbit it varies from L to R or R to L, the superstable point separating the two regions.

The MSS algorithm avoids the need for a separate search for stable periodic orbits of each period. Its basic step is to start with the U sequence complete up to some small period such as 3 or 4 and to interject LIPs with more symbols between each adjacent pair of LIP's already present. This is done by comparing the "harmonic extension" of the left-hand LIP of any pair with the "antiharmonic extension" of the right-hand LIP. The desired new LIP is the common left-hand end of the two sequences just defined. Here the *harmonic* of a LIP is two copies of the LIP separated by an R if the LIP has an even number of R's, and by an L if the LIP has an odd number of R's, and the *antiharmonic* uses the alternative separator. The *harmonic extension* is found by indefinitely iterating the procedure for finding the harmonic, and similarly for the *antiharmonic extension.* In effect, the harmonic (which is a LIP) must lie to the right of its originating sequence on the parameter line, and the antiharmonic must lie to the left of its originator. The antiharmonic is not a LIP but, as we now can show, can generate LIP's of interest. As an example, the sole period-3 LIP is RL, its harmonic is $RL(L)RL$, and the next stage in its harmonic extension is $RL(L)RL(R)RL(L)RL$, where we have put parentheses around the separator symbols. The antiharmonic of the period-3 LIP is $RL(R)RL$, and the next stage in its antiharmonic extension is $RL(R)RL(R)RL(R)RL$. It is easy to see that the complete antiharmonic extension of period 3 is $RLR^2LR^2LR^2\ldots$, a periodic symbol sequence.

Rather than looking for the entire U sequence, we concentrate on the range of μ just below the stability range of period 3. We know that the U sequence, complete to period 4, in our region of interest, is RLR,RL. A MSS search between these LIP's finds RLR^2 (5), where the period of the related periodic orbit is in parenthesis. Iterating this procedure, we now look between RLR^2 and RL, and find RLR^2LR (7). Then in succession we find RLR^2LR^2 (8) and RLR^2LR^2LR (10). It is clear that these LIP's are all truncations of the antiharmonic extension of the period-3 LIP, and that this process can be continued indefinitely. It finds periodic orbits having ever longer periods with parameter stability ranges ever close to that of period 3. These orbits have periods $3n+1$, and $3n+2$, $n=1,2,\ldots$ (or LIP's with $3n,3n+1$ symbols). Once we pass the tangent bifurcation value of μ for one of these orbits, all stable periodic orbits occurring before the period-3 tangent bifurcation have at least as many symbols of the antiharmonic extension of the period-3 LIP as that orbit. Truncations of the antiharmonic extension of period 3 that would give periods that are multiplies of 3 are excluded, because they are not LIP's. Further exclusions occur among possible precursor orbits to higher period intermittencies and will be discussed in Sec. V. Table I shows the tangent bifurcation values of μ for the orbits that we have just described up to period 41, and the widths of the stability windows of these orbits. The occurrences of the precursor stable periodic orbits are in accord with the $\epsilon^{-1/2}$ behavior of the average lengths of the periodic intermittent bursts, and thus afford a microscopic view of that phenomenon.

A related point in phase space concerns the positions of the orbit points of a 3-mimic as its period increases. Because of their symbolic dynamics, the orbit points clump in three groups related to the incipient intervals of period-3 activity. Consider the superstable case: One orbit point must be $y=0.0$. As the period increases, ever more orbit points crowd into the region that is reserved for period-3 activity. In Table II we show the orbit points in the central clump for superstable period 41.

TABLE I. Tangent-bifurcation ($s_{n<3}$) and window-destroying ($h_{n<3}$) values of μ, and window widths ($\Delta\mu_{n<3}$) for 3-mimic orbits at $J=0$. Here $n<3$ means the orbit of period n with the closest stability range of μ below $s_3=1.75$, the limiting value in the table as n increases.

Period (n)	$s_{n<3}$	$h_{n<3}$	$\Delta\mu_{n<3}$
5	1.624 397	1.633 36	0.008 96
8	1.711 037	1.711 42	0.000 39
11	1.732 001	1.732 049	0.000 048
14	1.739 716 4	1.749 727 8	0.000 011 4
17	1.743 337 4	1.743 341 3	0.000 003 9
20	1.745 319 4	1.745 321 1	0.000 001 7
23	1.746 523 3	1.746 524 1	0.000 000 8
26	1.747 310 7	1.747 311 2	0.000 000 5
29	1.747 854 9	1.747 855 3	0.000 000 3
32	1.748 247 4	1.748 247 7	0.000 000 2
35	1.748 540 2	1.748 540 3	0.000 000 2
38	1.748 764 6	1.748 764 7	0.000 000 1
41	1.748 940 5	1.748 940 6	0.000 000 1

They move out of the period-3 region in time for the next 3-mimic to take a superstable position. We will refer to this point in a later discussion of the case $J>0$.

It is also of interest that, in accord with the numerical findings of Lorenz near $\mu=2.0$, the parameter range having *some* stable periodic attractor in the intermittent range preceding period-3 stability is very small numerically. This explains why, in real and computer experiments, the course of intermittency with parameter increase never seems to be interrupted by other stable periodic windows.

As a technical point it is worth noting that, because of Singer's theorem, the most straightforward numerical method for finding the stability windows of periodic orbits at $J=0$ is to calculate the Lyapunov exponent from any starting point in the trapping region as a function of μ. Because stability windows tend to be narrow (see Table I), in order to find one it is helpful to have some idea of its width as well as of its (approximate) location in μ, the latter being available from its MSS sequence by a rapidly convergent technique [12].

III. SOME GENERAL FEATURES OF $J>0$ MAPS

There are many clues to the changes that are found in intermittency as J is increased from zero. Although there is overlap in their contents, they all represent different insights, and as such are potentially useful in studies of ever more complicated maps. We consider events both in parameter space (J,μ) and phase space (x_n,y_n). These are static plots. It would be even more useful to make a four-dimensional (4D) plot of $(x_{n+1},y_{n+1};x_n,y_n)$ which would correspond to the extremely revealing plot of y_{n+1} vs y_n for the quadratic map, which enables us to trace the time evolution of any starting point by eye, but human limitations intervene. As proved by Holmes and Whitley [6], the saddle-node loci in parameter space, $\mu=s_{n,k}(J)$, for every n and k, are continuous curves from $J=0$ to 1, although each line may cross both itself and all of the others. Many other important loci exist in parameter space, signifying other important topological dynamical events, among which are period-doubling bifurcations, and different homoclinic and heteroclinic bifurcations. Figure 2, taken from Ref. [6], shows plots of some important bifurcations that appeared in that reference. We will have occasion to introduce a further set of homoclinic bifurcations that is crucial to our particular concern with the evolution of intermittency. Before doing this, it is useful to sketch the underlying concomitant events that occur in the phase space.

TABLE II. Orbit points of the period-41 3-mimic orbit at $(J,\mu)=(0,1.748\,940\,483)$ associated with the central period-3 orbit point.

0.000 000	0.033 227	0.043 326
0.050 376	0.056 386	0.062 212
0.068 471	0.075 862	0.085 472
0.099 380	0.122 287	0.166 959
0.277 270	0.653 043	

We are concerned with the stable and unstable manifolds that accompany every periodic point whether or not it is stable. The limiting 1D case has simplifying features, the connected kernels of which are the one-hump feature of the map and its double-valued inverse. The 1D map, when limited to the portion of the abscissa y_n for which $-A<y_n<y_{n+1_{\max}}$, is the analog of the *important* branch of the unstable manifold (UM) of the unstable fixed point of the Hénon map at $(x,y)=(-A,-A)$, where $A=(\frac{1}{2})(1+J+[(1+J)^2+4\mu]^{1/2})$. [The other branch of the UM lies outside the trapping region for all (J,μ) and

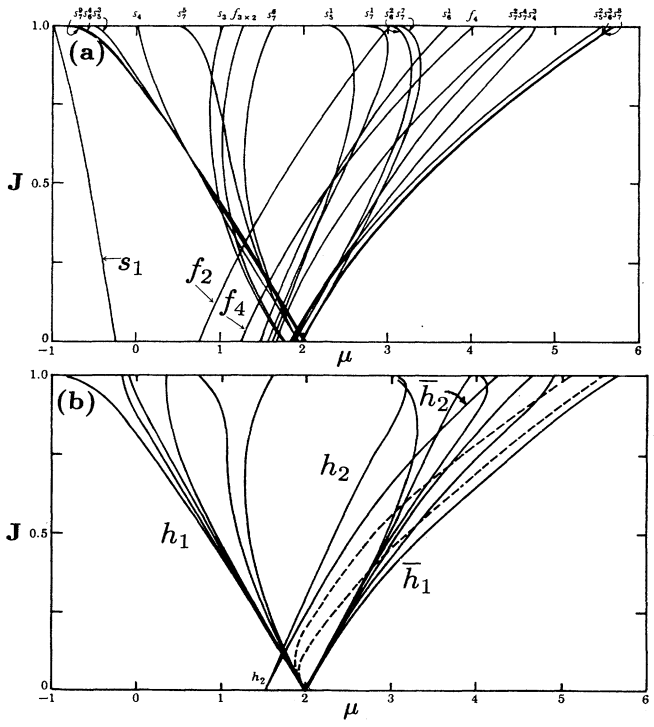

FIG. 2. Some bifurcation curves for the Hénon map. (a) Saddle-node bifurcations (s), and period-doubling bifurcations (f), for periods $n\leq 7$. (b) Homoclinic bifurcation curves. (This figure is reproduced from Ref. [6] with the permission of the author and of the Royal Society of London.)

goes monotonically to infinity.] It is referred to below in a discussion of homoclinic tangency. Note that, for all J, the UM is intimately connected to the location of the strange attractor(s) which exist for a finite measure of parameter values. At $J=0$ the stable manifold (SM) of $(-A,-A)$ is just an infinite horizontal line through that point, and an infinite line through the point $(+A,+A)$. These "join at $x\to+\infty$."

Once we leave $J=0$, a profound change takes place: The map is invertible, the inverse mapping being given by

$$x_n=(1/J)(\mu-y_{n+1}-x_{n+1}^2),\quad y_n=x_{n+1}\ ,$$

where the factor $1/J$ shows explicitly why all SM's of fixed and periodic points are horizontal lines for $J=0$. The SM of $(-A,-A)$ is the border of the trapping region. The UM of $(-A,-A)$ is a curve which, for $\mu>J-J^{1/2}(1+J)$, a value not far above the saddle-node value $s_1(J)=-(1+J)^2/4$, spirals around the only other fixed point $(+B,+B)$ an indefinitely large number of times, or past homoclinic tangency follows an even more tortuous path. Here $B=(\frac{1}{2})(-(1+J)+[(1+J)^2+4\mu]^{1/2})$. The UM has many critical points (i.e., maxima and minima). Singer's theorem no longer applies because each of many critical points may harbor a periodic orbit and its BA, and so multistability is the order of the day. The extreme case is at $J=1$, for which, although one cannot speak of attractors and BA's, there is an infinite number of elliptic island chains for the largest measure of values of μ for which a trapping region exists. The occurrence of multistability and the relation of this to intersections, or not, of various invariant manifolds is closely tied to the changes that occur in intermittency. For the most part we will be interested in very small positive values of J, which will afford us some simplification because of similarity to the case $J=0$. However, some understanding of the complex features of the bifurcation curves in Fig. 2 is helpful because these affect the course of intermittency associated with various periodic orbits.

Just as the trapping region is bounded by the SM of $(-A,-A)$, so each (n,k) BA is bounded by the SM's of the unstable periodic-orbit points on its boundary. The vagueness of this definition can be avoided by treating J values appropriately close to zero, thus avoiding metamorphic basin boundary jumps [13,14]. With this restriction, the bounding SM's belong to the unstable n-periodic-orbit points which appear at the (n,k)-saddle-node bifurcation. Just as BA's are formed at saddle-node bifurcations, so BA's are destroyed at heteroclinic bifurcations or tangencies. Some related homoclinic tangency or bifurcation lines are seen in Fig. 2(b). We refer to these as *h type* to distinguish them from another group that will be introduced below. In particular note that a group of such loci, or lines, known as a *homoclinic fan* leave the point $(\mu,J)=(2.0,0.0)$ [6]. This point is known in the 1D case as (the first) Misiurewicz point [4], a limiting endpoint for a very large number of saddle-node bifurcations, which is also the upper limiting parameter value for the existence of a trapping region. It is clear that a Misiurewicz point is very degenerate from a topological point of view, and that some of the degeneracy is removed when $J>0$. To be clear about definitions, a homoclinic tangency or bifurcation occurs at a parameter pair at which the SM's and UM's of a fixed point or periodic point are tangent, and a heteroclinic tangency occurs at a tangency of a SM and a UM of distinct periodic-orbit points. Parameter pairs of a particular tangency vary along curves in parameter space which are continuous from $J=0$ to 1. Such tangencies were first introduced in the study of Hamiltonian, or area-preserving systems [15]. The relative simplicity of the very large dissipation limit ($J=0$) can be looked at as the gradual degeneration of h-type homoclinic tangency as J decreases from 1 to 0 so that, at $J=0$, it is confined to the Misiurewicz points which only occur at the set of parameter values at crises, at which strange attractors exist [16].

If Figs. 2(a) and 2(b) were superposed, one would notice that many saddle-node bifurcation lines cluster in the vicinity of various homoclinic tangency lines. We will concentrate on the first (i.e., leftmost) homoclinic line $h_1(J)$, and the last homoclinic line $\bar{h}_1(J)$, leaving the Misiurewicz point (0,2) [4]. We notice that a set of saddle-node bifurcation lines: $s_3(J)$, $s_4(J)$, $s_{5,3}(J)$, $s_{6,4}(J)$, and $s_{7,9}(J)$, and an infinite number of others, one for each period, leave $J=0$, and follow ever closer along the course of $h_1(J)$ as the period increases. In each case the saddle node $s_{n,K}(J)$ is the last saddle node $s_{n,k}(J)$ of period n in the MSS sequence (at $J=0$), with symbol sequence RL^{n-2}. We note here, for future use, that the work of Biham and Wenzel [17] and some of our own calculations support the conjecture that the symbolic dynamics of every periodic orbit can be taken the same for all real, and even complex! J and μ, when used with the Biham and Wenzel algorithm for finding periodic orbits, assigning $R=+1$ and $L=-1$. This despite the fact that for $J>0$ the MSS ordering of symbol sequences for constant J is only fortuitously valid. At $J=1$, the $s_{n,K}(J)$ have all crossed $h_1(J)$, and occur in inverse periodic order with increasing J. The crossing are essential because the nature of the area-preserving limit requires that $h_1(1)=s_1(1)$, and no trapping region exists for $\mu<s_1(1)$. The intuitive reason that these orbits remain close to $h_1(J)$ is that the orbit points follow clockwise around a topological circle, as seen in Fig. 3(a) in a very similar way to that in which the homoclinic tangency points proceed at $h_1(J)$, as seen in Fig. 3(b). Each of these saddle nodes occurs at a resonant bifurcation, a typical area-preserving phenomenon, and its BA survives for a range of μ that is much larger than one's expectations from its behavior at $J=0$ [5–7]. The reversal of the μ order of these orbits between $J=0$ and 1 can be understood on dynamical grounds in terms of the struggle between nonlinearity and dissipation. In the area-preserving case there is no dissipation, and an orbit in which a small change occurs in one time step is similar to a long-wavelength mode of a string. For example a period-9 orbit completes a circle in nine time steps while a period-3 mode goes around three times in nine time steps, like a string mode with three nodes. By contrast, at $J=0$, dissipation is strong and only to go around a circle one time in a large number of steps requires very large nonlinearity to counteract the very large dissipation, according to Schuster's driven damped rotator model of the

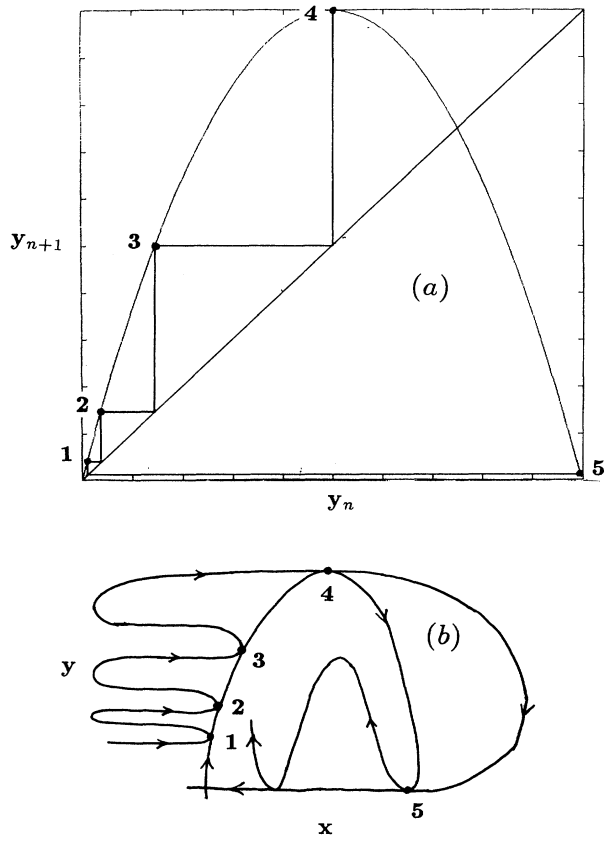

FIG. 3. (a) The MSS construction of the periodic-orbit points for $(n,k)=(6,4)$. (b) A schematic diagram showing the *first* homoclinic tangency of the stable and unstable manifolds of the unstable fixed point. Note that the positions of the tangency points resemble those of the periodic-orbit points in Fig. 3(a).

Hénon map [3].

Now, for contrast, look at the last homoclinic tangency $\bar{h}_1(J)$, which for all J just precedes the formation of a complete Smale horseshoe [18],[6] which destroys the trapping region. For each period n, the saddle node which closely follows this homoclinic line is the next-to-last one in the MSS sequence: $s_{n,K-1}(J)$. The symbol sequence in this case is $RL^{n-3}R$. Figure 4(a) shows a typical orbit among this set, and Fig. 4(b) shows the quite similar last homoclinic tangency. Because of the Smale horseshoe formation at $\bar{h}_1(J)$, none of these saddle nodes can cross it. The dynamical reason for the extremely large difference $\bar{h}_1(1)-h_1(1)\cong 6.8$ is not so clear. Tentatively one may say that putting in a single loop of length 2 into a long small-amplitude loop creates a large tension in an area-preserving system, while for a dissipative system it does not change the important largest amplitude by very much, as long as the orbit is sufficiently long.

Homoclinic tangencies play equally important roles for higher-period BA's, with one important difference. In the period-1 case, when considering $\bar{h}_1(J)$, the entire trapping region is at stake, because a point outside of it will rapidly approach the ever present attractor at infinity. In this connection we noted above that the other half of the unstable manifold of $(-A,-A)$ goes straight to infinity, so that it can never return and cause a homoclinic tangency with the other half of the stable manifold. As a generalization, h-type homoclinic tangency, for a periodic orbit with $n\neq 1$, always involves the half of the UM of an unstable periodic-orbit point of period n that lies in the n-BA. If the n-BA is created at a saddle-node bifurcation, and $n\neq 1$, then the other half of the UM varies independently, and unless the n-BA is surrounded by the basin at infinity (which can happen once the 1-BA, or some other enveloping BA, no longer exists) this second UM branch may also take part in a homoclinic tangency or intersection. We call this an h'-type homoclinic tangency. For example, many higher-period BA's of period n which are born at saddle-node bifurcations, at least at values of μ for which the period-1 BA exists (to be given below), have the other halves of the unstable manifolds of the unstable period-n points existent in the period-1 BA. Because of the overriding attracting properties of the unstable manifold of the point (B,B) intrinsic to the Hénon map for any parameter pair, the period-

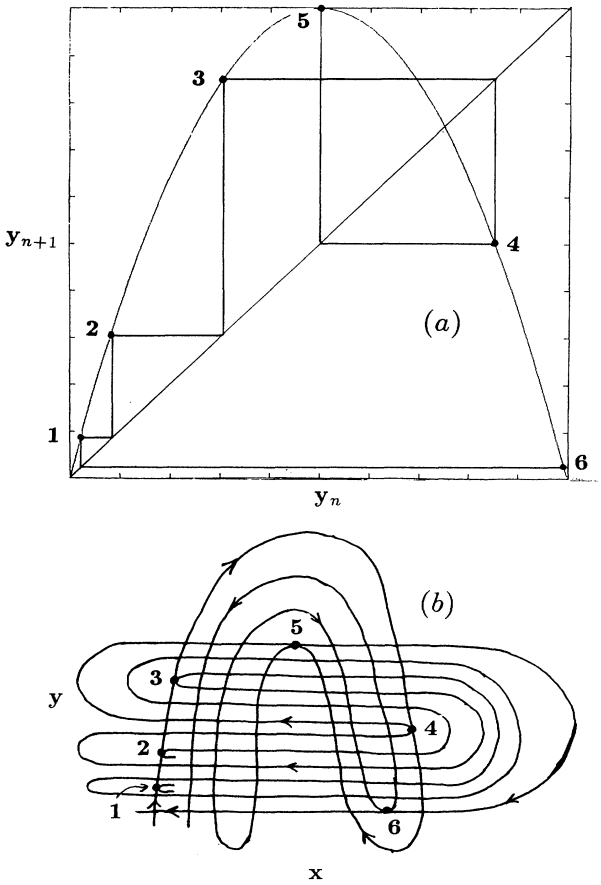

FIG. 4. (a) The MSS construction of the periodic-orbit points for $(n,k)=(6,3)$. (b) A schematic diagram showing the *last* homoclinic tangency of the stable and unstable manifolds of the unstable fixed point. Note that the positions of the tangency points resemble those of the periodic-orbit points in (a).

n unstable manifolds approach the (B,B) UM in the long-time limit. A particular case of some relevance for our treatment of intermittency in the simple case of period 3 is shown in Fig. 5. We pick a parameter pair (0.2,1.33) that is not near intermittency because it shows the approach of the two UM's of concern without the extra complications inherent in intermittency. Note that $s_3(0.2)=1.32$ and that at (0.2,1.33), $A=1.9$, $B=0.7$, and the period-3 BA contains a period-3 point attractor

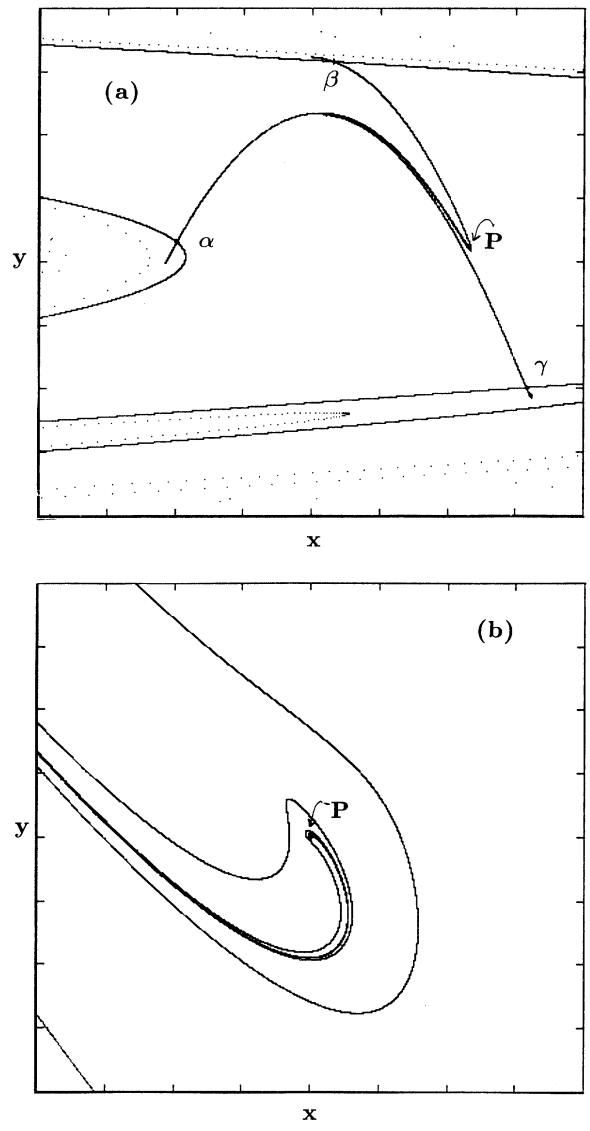

FIG. 5. (a) The stable and unstable manifolds of the period-3 unstable periodic-orbit points marked α,β,γ, which lie on the boundary of the period-3 basin of attraction. Here $(J,\mu)=(0.2,1.33)$. The stable period-3 orbit points are at the apparently abrupt ends of the parts of the unstable manifolds in the period-3 basin of attraction. Point P is a period-2 fixed point, and is close to the period-1 unstable manifold which is gradually approached by the period-3 unstable manifolds. (b) A blowup showing the wrapping of the period-3 unstable manifold branches around point P in (a). The linear magnification (b) relative to (a) is 312.5 in both directions.

at successive cyclic pairs of the values $(-1.018\,83, -0.014\,721, 1.497\,53)$. Figure 5(a) shows the important parts of the period-1 and period-3 BA's in a phase plane plot (x_n,y_n) with its center at (0.0,0.0). The fixed point $(-A,-A)$ is at the lower-left-hand corner. The period-3 unstable periodic points are successive cyclic pairs of the set of three values $(-0.941\,55, 0.143\,97, 1.497\,56)$. They are marked α,β,γ, and the stable and unstable manifolds through them are noted. The region inside the innermost stable manifold branches is the main part of the period-1 BA and contains a period-2 point attractor at the points (x_n,y_n) given as (0.1,1.1) in either order. The period-2 attractor points are surrounded by the UM of (B,B). The parts of the unstable manifolds of α,β,γ in the period-1 BA are gradually converging to the UM of (B,B). Figure 5(b) shows the region near the rightmost period-2 attractor point [labeled P in Figs. 5(a) and 5(b)] magnified in both directions by factors of 312.5. The period-2 attractor point at (1.1,0.1) is in the center of the figure. The outermost curve originates at point α, the next at β, and the next at γ. The inner folds of these are not distinguishable from each other or from the UM of (B,B). All of the period-3 UM's cycle clockwise, but the entire group appears to cycle counterclockwise about the period-2 point because the UM of (B,B) cycles counterclockwise. This is consistent with the cycling of orbits in island chains in the area-preserving limit. As μ increases, the UM of (B,B) develops folds preliminary to homoclinic tangency with the (B,B) SM, and, after that tangency, eventually approaches and intersects the SM's of α,β,γ; *concomitantly, the homoclinic tangency* $h_3'(J)$ *must occur.* This shows the conditions in which homoclinic tangency and intersection of the period-3 manifolds develops. Homoclinic intersections of this type were not discussed in Ref. [6], but are crucial to a discussion of intermittency for Hénon maps. They are also the key to a discussion of metamorphosis, or discrete change in a basin boundary [13,14]. We define the value of μ for which homoclinic tangency of the kth MSS orbit of period n occurs in parameter space as $h_{n,k}'(J)$. We stress that this is a homoclinic tangency involving the branches of the UM's of period n in the surrounding BA out of which the period-n BA is sculpted. It is distinct from $h_{n,k}(J)$, which involves the UM branches that leave the period-n unstable periodic-orbit points within the period n-BA (when this BA is stable). We will see that the existence of the locus $h_{n,k}'(J)$ is not guaranteed for all values of J.

IV. INTERMITTENCY OF PERIOD 3

A. Computational results

As a first, and arguably the most important, case of type-I intermittency, we study that related to the existence of a period-3 attractor. At $J=0$ the standard picture, described in Sec. II, is that for most values of ϵ near and preceding s_3 there is a strange attractor, but as $\epsilon\to 0$, its Lyapunov exponent decreases to zero. We can relate this to the existence of homoclinic *intersection* of the h' type at $J=0$. Figure 6 shows the UM of $(-A,-A)$ at

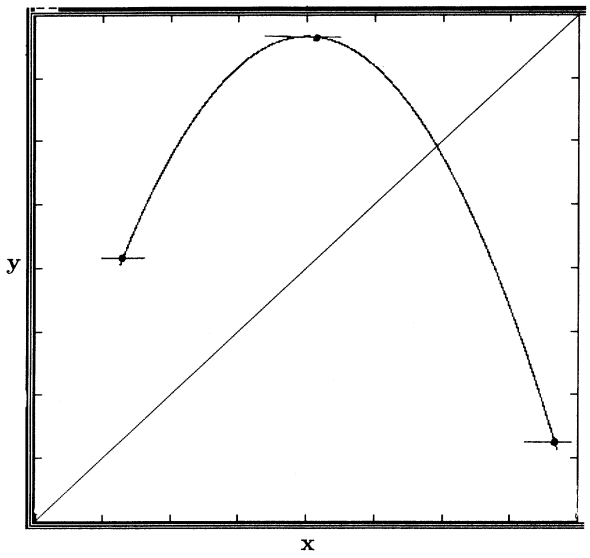

FIG. 6. The intersection of the period-3 stable manifold branches with the period-1 unstable manifold at $(J,\mu)=(0,1.75)$. These intersections explain why bistability of the period-1 and period-3 basins of attraction is not possible at $J=0$. Elaborating on accepted terminology, the removal of the barrier to bistability at $J=J^*(3)$ might be called *crisis resolution.*

$J=0$ for $\mu=s_3=1.75$. The UM of (B,B) lies along the same parabola, and if there is a strange attractor it must be dense along this UM. We also mark the three period-3 fixed points on this manifold, and through each of them we draw a horizontal line which is part of its SM. Certainly each horizontal line crosses the UM parabola. If period-1 and period-3 BA's were bistable, this crossing could not occur because the period-1 BA has a strange attractor in it just preceding s_3, and could be expected to continue to do so as μ increases. Because the period-3 UM wraps tightly around the (B,B) UM, this means that period-3 h'-type homoclinic intersection exists. In combination with the existence of a finite-μ interval of stability, $\Delta\mu(3)\equiv h_3-s_3$ of the period-3 BA before h_3 occurs, we can see why the period-3 BA destroys the period-1 BA when $\mu=s_3$. As J increases, $s_3(J)$ decreases because it follows along with $h_1(J)$ so that it can take its rightful place as a resonant bifurcation evolving within the period-1 elliptic basin at $J=1$, starting at $\mu=s_3(1)=1.0$. Concomitantly the folds of the $(-A,-A)$ and (B,B) UM's separate in such a way that the h'-type homoclinic intersection is gradually withdrawn leading to a homoclinic tangency $h_3'(J)$, and then withdrawing all contact of the UM and SM of period 3. The smallest value of J at which $h_3'(J)$ occurs is $J^*(3)=0.001\,15$. This is one coordinate of a codimension-2 point in parameter space. Using the result of Hitzl [19], $s_3(J)=(\frac{1}{4})(7J^2-10J+7)$, the corresponding value of μ is 1.747 13. We have established numerically that $h_3'(J)$ exists for $J^*(3)\le J<1.0$. This is done by plotting the two manifolds and adjusting μ and J to the five-place accuracy shown here, so that tangency just exists. An analytic approach to the tangency problem would be very difficult because of the multivaluedness of the manifolds. The course of $h_3'(J)$ is complicated and will be discussed elsewhere. In Fig. 7, we show $s_3(J)$, $h_3(J)$, and $h_3'(J)$ in the parameter plane for a range of values of interest for the development of type-I period-3 intermittency. The numerical values of interest are noted, but the values are not to scale in this qualitative figure because they are clumsily disparate in size. Note the crossing of $h_3(J)$ and $h_3'(J)$, at the codimension-2 point defined as $J'(3)$, which will be discussed below. For J shown between 0.0 and 0.02, the period-3 BA exists with some attractor for $s_3(J)\le\mu\le h_3(J)$. We now turn to the form that period-3 intermittency takes in this range of J.

The numerical tools that we use to study period-3 intermittency for each Hénon-map subfamily with $J>0$ are the same as those used above for $J=0$, namely the time trace, the Lyapunov exponent, and the orbit density of an initial point which starts in the period-1 BA. We have found that a very satisfactory initial point for all of these calculations is one very close to (B,B); such a point is unlikely to be in any BA other than that of period 1. Because we are only interested in the long-time behavior, we always ignore initial transients by preiterating for anywhere between 10^4 and 10^5 iterates. For $J<J^*(3)$, the results differ only in part from those at $J=0$: the time trace continues to show an increase in the fraction of regular behavior as $\epsilon\equiv s_3(J)-\mu\to 0$, with the average length of a regular burst varying as $\epsilon^{-1/2}$, and the Lyapunov exponent varies as $\epsilon^{1/2}$. Furthermore, for a reason soon obvious, the parameter range in which the intermittency occurs decreases. The significant harbinger of important change is that the orbit density of the intermittent peaks

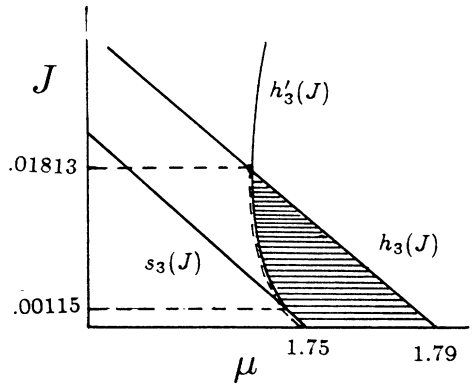

FIG. 7. Bifurcation lines relevant to the stability conflict between period-1 and period-3 basins of attraction (BA's). Other (n,k) BA's are ignored. The period-3 BA is stable between $s_3(J)$ and $h_3(J)$. The period-1 BA is stable to the right of $h_3(J)$, and to the left of $h_3'(J)$ if $J>0.001\,15$, and to the left of $s_3(J)$ if $J<0.001\,15$. Intermittency potentially occurs immediately to the left of this line, indicated by dashes, defining the destruction of the period-1 basin, but only if the period-3 basin exists $(J<0.018\,13)$. In the shaded region, the period-1 BA has been swallowed by the period-3 BA.

gradually becomes more asymmetric as J increases. However, the integrated fractional density under each of the three peaks remains unchanged for parameter pairs correspondingly close to $s_3(J)$. Note that, for $J>0$, we consider a 1D density: the orbit projected on $x_n=0$. (We could as well have projected the orbit on $y_n=0$ because of the equation $x_{n+1}=y_n$.) In two dimensions, the orbit density is expected to be fractal along a direction perpendicular to the main UM with a very narrow total width. The numerical results for this more elaborate density, although of theoretical importance, are not of interest in the present discussion; our concern is a comparison with the invariant density in the limit $J=0$. We have assumed, along with most physicists, that SA's exist for the 2D case, and that their properties parallel those of the better-established 1D SA's, including, in this case, the existence of an invariant 1D projected orbit density. Operationally the 1D density may be thought of as a sum of contributions from all of the fractal branches of the 2D density.

More interesting changes occur for $J>J^*(3)$. Figure 8 shows the time traces of orbits for the three parameter pairs $(J,\mu)=$(a) (0.0011,1.747 251 0), (b) (0.0012,1.747 004), and (c) (0.0015,1.746 352). There are three "time lines" (horizontal) in each diagram. The solid lines on the sides of each time line indicate the coordinate value (vertical) of zero. In each case an increase of 10^{-6} in μ will destabilize the period-1 BA. The continuing decrease in regular period-3 behavior as J increases above $J^*(3)$ is apparent. Figures 9(a)–9(c) show the Lyapunov exponent of an orbit which starts in the period-1 BA as a function of small ϵ for the same values of J as in Fig. 8. We see that the Lyapunov exponent, *a statistical quantity* undergoes a first-order rather than a continuous-phase transition when ϵ goes through zero and $J>J^*(3)$. In addition, one begins to see what is more apparent at still larger values of J, that the transition is then to a negative value of λ, *rather than to* $\lambda=0$. Note that in all three cases $\lambda\simeq 0.375$ when $\epsilon\simeq 0.000\,75$. Finally, the smallest values of λ for $\epsilon=2\times10^{-7}$ are approximately 0.04, 0.20, and 0.30, respectively. Figures 10(a)–10(c) show histograms of the change in the invariant orbit density of the y (or x) coordinate near the cen-

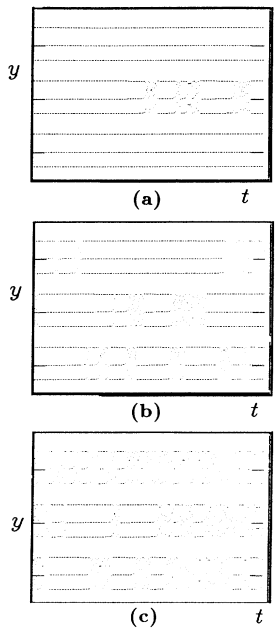

FIG. 8. (a)–(c) The time traces of orbits for $(J,\mu)=$(a) (0.0011,1.747 251), (b) (0.0012,1.747 004), and (c) (0.0015,1.746 352). In all cases, $\epsilon=10^{-6}$, where, in (a) $\epsilon\equiv s_3(J)-\mu$, while in (b) and (c) $\epsilon\equiv h_3'(J)-\mu$.

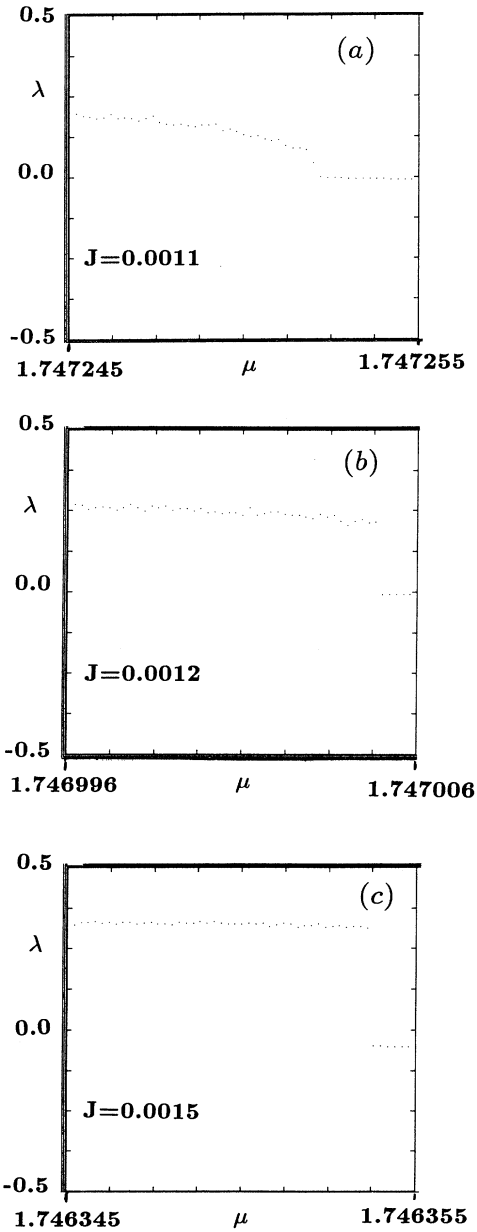

FIG. 9. (a)–(c) The Lyapunov exponent $\lambda_J(\mu)$ as a function of μ for (small) ϵ, and the same values of J as in Fig. 8. The change from a continuous to a first-order phase transition for $\lambda_J(\mu)$ when J exceeds 0.001 15 is apparent.

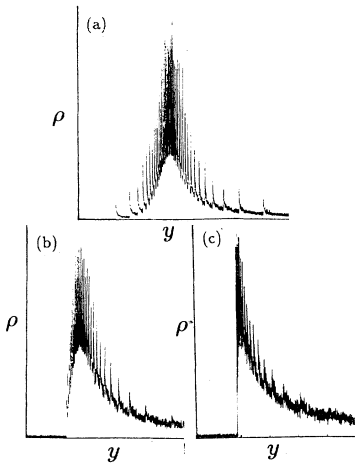

FIG. 10. (a)–(c) Invariant orbit densities for the y (or x) coordinate near the central period-3 peak for $J=0.0$, 0.001, 0.0015, and the illuminating value $\epsilon\simeq 10^{-5}$. In each of these plots the normalization is to the largest histogram value, so relative areas are not evident.

tral period-3 peak for $J=0.0$, 0.001, and 0.0015, and $\epsilon\simeq 10^{-5}$. In each case the y range shown is divided into 2400 equal intervals. The gradual skewing of the peak as J increases is apparent. Because each peak is normalized to its largest vertical value, the decrease in peak area for $J>J^*(3)$ is not obvious. To remedy this defect, we note that for $J=0.0$, 0.001, 0.001 2, and 0.001 5, and $\epsilon=10^{-6}$, the area ratios are 2.82:2.81:1.82:1.37. The reasons for these changes can all be traced to the consequences of the codimension-2 point $(J,\mu)=(J^*(3),s_3(J^*(3)))$. Most of the arguments are qualitative, depending upon extrapolations of the arguments in Secs. II and III.

B. Explanation in terms of the codimension-2 point $(J^*(3),s_3(J^*(3)))$

The codimension-2 point $(J^*(3),s_3(J^*(3)))$, while not as degenerate as a Misiurewicz point, still is a limit in parameter space of a set of important topological events. The results of our topological arguments for $J=0$, and their numerical continuation for $J>0$ show, that the 3-mimic saddle nodes limit at $\mu=s_3(J)$ for $J<J^*(3)$. For $J>J^*(3)$, there is an unexpected split in the behavior of the 3-mimic saddle nodes: Those with periods of the form $3n+2$ continue to limit at the curve $\mu=h_3'(J)$ up to high values of J. We have checked this up to $J=0.95$ and periods up to 23. Those with periods of the form $3n+1$ cross $h_3'(J)$ in order of *decreasing* n as J increases. The codimension-2 point acts as the high-n limit for the $3n+1$ saddle-node crossings. This limiting behavior is probably a hallmark of its codimension-2 character. A number of the small-n crossings occur above $J'(3)$. The smallest-period crossing below $J'(3)$ is that of period 22 (i.e., $n=7$) near $J=0.018$. The crossing of period 7 is near $J=0.2$. Note that each $3n+1$ saddle node that has crossed $h_3'(J)$ has also crossed an infinite number of $3n+2$ saddle nodes. We do not completely understand this behavior in terms of manifold crossings. We merely note the suggestive topological fact that the LIP's of $3n+1$ orbits are even in R while the LIP's of $3n+2$ orbits are odd in R. Figure 11 shows the same bifurcation lines as in Fig. 7, supplemented by saddle-node bifurcation lines of some of the 3-mimics and some of the crossing points of $3n+1$ 3-mimics. This time the values are to scale. In Table III, we show approximate values of $s_n(J)$ for a few 3-mimic $(3n+1,3n+2)$ pairs for several values of n. In each case we use a value of J not far above that for which the $3n+1$ saddle node has crossed $h_3'(J)$. Most of our computer results for intermittency can be explained on this basis.

(1) Why intermittency occurs at $h_3'(J)$ rather than at $s_3(J)$: In Fig. 11, we see that, as J increases above $J^*(3)$, the 3-mimic saddle nodes abandon $s_3(J)$ and follow ever closer to $h_3'(J)$. Even though *some* of the $3n+1$-type 3-mimics cross this line, a discontinuity in intermittent behavior is to be expected upon crossing $h_3'(J)$ as a modification of the $\epsilon^{1/2}$ behavior of the Lyapunov exponent in the period-1 BA observed when $J<J^*(3)$. Thus there is a dynamic reason for period-3 intermittency to be associated with the temporary *destruction* of the period-1 BA [at $h_3'(J)$] rather than with the *creation* of the period-3 BA [at $s_3(J)$], these two events no longer being simultaneous with parameter variation when $J>J^*(3)$. We believe the reason for this is the same as the reason that some orbits follow close to $h_1(J)$ and others follow close to $\bar{h}_1(J)$, as discussed in Sec. III. Orbits which follow close to $s_3(J)$ for all J have symbolic dynamics resembling that of multiples of 3. The ones we

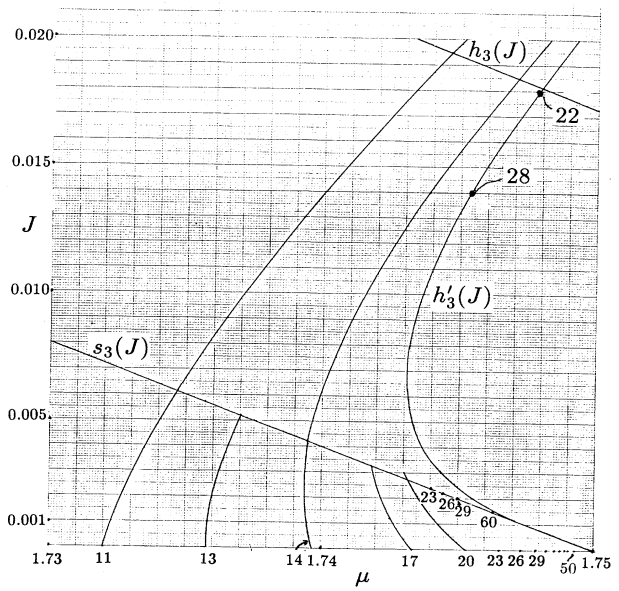

FIG. 11. The same bifurcation lines as in Fig. 7, but now to scale, and supplemented by saddle-node bifurcation lines of several 3-mimics, and points at which two $3n+1$ 3-mimics cross $h_3'(J)$. The latter are labeled by their periods, 28 and 22.

TABLE III. Saddle-node bifurcation values of μ for 3-mimic pairs $(3n+1, 3n+2)$, compared to homoclinic values $\mu = h_3'(J)$. The crossings of $h_3'(J)$ by the $3n+1$ saddle nodes shown are crucial to an understanding of the variation of the Lyapunov exponent with J above $J^*(3)$.

J	Period (n)	$s_n(J)$	Period (n)	$s_n(J)$	$h_3'(J)$
0.2	7	1.991 904	8	1.973 922	1.979 832
0.02	19	1.749 31	20	1.749 15	1.749 27
0.014	28	1.745 43	29	1.745 32	1.745 386

are concerned with here are truncations of the antiharmonic extension of period 3, *excluding the multiples of 3* (none of which are LIP's). It is dynamically reasonable to expect that if $s_3(J)$ goes upwards to the left, then $h_3'(J)$ will go upwards to the right, if only because the 3-mimics which limit at it have orbit points that more nearly resemble the tangency points of $\bar{h}_1(J)$ rather than those of $h_1(J)$ (see Figs. 3 and 4). Between $s_3(J)$ and $h_3'(J)$, we find that the 3-mimic BA's are bistable with the period-3 BA, probably because their qualitatively different symbolic dynamics does not allow any intermittency in the transition between them. It is not clear whether this relative stability continues to hold between $h_3'(J)$ and $h_3(J)$, but, as remarked in Sec. II concerning $J=0$, the effect on intermittency will be minimal because the parameter stability ranges of the 3-mimic BA's are very small.

As far as calculation is concerned, in the parameter range of concern we are fortunate that the period-1 BA is unstable with respect to each of the 3-mimic-period BA's, so that an initial point near (B,B) iterates to the attractor in the 3-mimic BA while that BA is stable. This is consistent with the idea that, as dissipation is increased from zero, high-period attractors approach their limiting dissipative behavior, defined as qualitatively similar to the behavior at $J=0$, after fewer *cycles*: We assume that the dissipation per cycle must reach a critical value of order 1 to achieve limiting dissipative behavior, and the dissipation per iteration is constant on the average. Thus we usually find that $J^*(n_1,k_1) > J^*(n_2,k_2)$ if $n_1 > n_2$, and the symbolic dynamics of the two orbits are similar. (Two examples of "similar" are period-3-mimics, and the last orbit of each period). Some indication of the irregularities in J^* values caused by k dependence appear in Sec. V. However the small parameter range of stability of the high-period BA's makes them hard to find even with a Lyapunov exponent search. A search using the method of Biham and Wenzel [17], which does not depend upon convergence of the Hénon dynamics of the orbit in question, is also not easy to apply when the orbit in question is stable, but is probably the best method available.

One result of the $s_3(J), h_3'(J)$ separation is that, if μ is varied slowly from a point to the left of $s_3(J)$ to a point to the right of $h_3'(J)$ and then reversed back to its starting point, *hysteresis* is likely to occur: An initial point will most likely be in the period-1 BA when $s_3(J)$ is crossed, and will stay in that BA until $h_3'(J)$ is crossed. When μ decreases from a value between $h_3'(J)$ and $h_3(J)$, a return to the period-1 BA will not occur until $s_3(J)$ is crossed. The hysteresis range is not great; it must be less than the μ width of the period-3 BA, which is about 0.4.

(2) Why there is a decrease of the Lyapunov exponent to a negative value when the period-1 BA is destroyed : The explanation is contained in Fig. 11. For $J^*(3) < J < J'(3)$, we see that $s_3(J) < h_3'(J) < h_3(J)$, and so at the transition the attractor in the period-3 BA can be anything from a period-3 orbit to a period-3 strange attractor. This is reflected in the first value of the Lyapunov exponent seen when the period-1 BA is swallowed by the period-3 BA.

(3) Why the μ range of intermittency decreases as J increases : In accord with the idea alluded to in Sec. I, Fig. 11 shows that the μ range of intermittency decreases with increasing J, because each 3-mimic saddle node approaches ever closer first to $s_3(J)$ and then to $h_3'(J)$ with increasing J, and it is the distance from a given 3-mimic to $h_3'(J)$ that determines where the Lyapunov exponent lies on the $\epsilon^{1/2}$ curve.

(4) Why there are changes in the orbit density : The existence of $h_3'(J)$ for $J > J^*(3)$ means that, because of its intimate proximity to the period-3 UM, the (B,B) UM, along which the strange attractor in the period-1 BA ranges, no longer intersects the period-3 SM, which acts as the period-1–period-3 basin boundary; thus period-1–period-3 bistability exists for $s_3(J) < \mu < h_3'(J)$, with hysteresis, as long as $h_3'(J) < h_3(J)$. Three further points must be explained: the shortened regular bursts in a time trace, and the decreased intensity and increased asymmetry of the orbit density peaks, the latter for all $J > 0$.

We address the last point first. In Fig. 12, we show stable and unstable manifolds of the central period-3 unstable-orbit point near that point (labeled Q), for $(J,\mu) = (0.001\,15, 1.747\,127\,3)$, a point very near to the

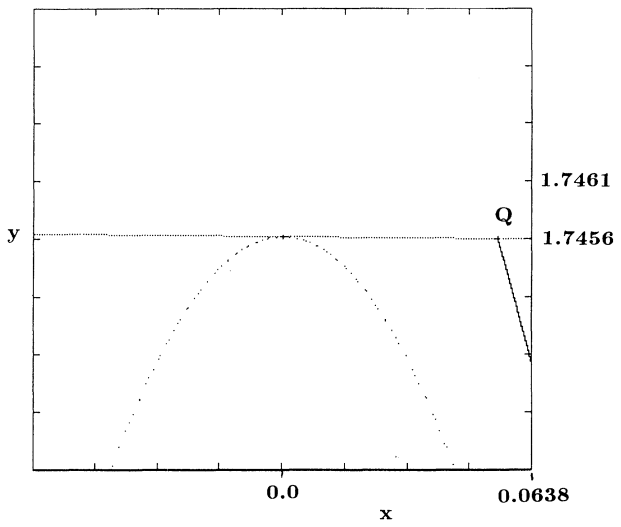

FIG. 12. Stable and unstable manifolds of the central period-3 unstable-orbit point near that point, for $(J,\mu) = (0.001\,15, 1.747\,127\,3)$. Here Q is the central period-3 unstable-orbit point.

codimension-2 point, $(J^*(3), s_3(J^*(3)) = h'_3(J^*(3)))$. The nearly horizontal line that slants slightly downwards to the right is the stable manifold, while the other lines belong to the branch of the unstable manifold in the period-1 BA. The vertical scale has been magnified by a factor of 1000, and the horizontal scale by a factor of 30, compared to a plot at the scale of the original equation. Consideration of small variations in this diagram can explain many features of maps near the codimension-2 point. This parameter pair is very near to several parameter pairs: (a) $J=0, \mu=1.75$; (b) $J=0.0007$, $\mu=1.748\,250\,9$; (c) $J=0.001\,15, \mu=1.747\,127\,4$; (d1) $J=0.002, \mu=1.745\,007$; and (d2) $J=0.002, \mu=1.745\,507\,0$. All cases except (d2) are at period-3 saddle-node bifurcations. (d2) is a point of h' homoclinic tangency. Among these, h'-type homoclinic intersection exists in (a) and (b), resulting in the SM crossing both visible branches of the UM. The homoclinic tangency of (c) looks just like the figure, while in (d1) homoclinic tangency has not been reached and the SM will appear above the central UM lobe. The right-hand piece of the UM has a very large number of unresolved branches, one of which must start at the periodic-orbit point. Consider case (d). The period-3 manifolds come into existence in (d1). By the time we increase μ from (d1) and reach (d2), the BA's of many $3n+2$ 3-mimics and many $3n+1$ 3-mimics will have come and gone, all bistable with the period-3 BA during their tenures of stability. It can be verified numerically that the images of an initial point near but below the critical point of the (B,B) UM, at the center of the diagram, all visually lie along the period-3 UM, *but to the right of the period-3 orbit point.* Of course the (B,B) UM and the existent 3-mimic UM's are visually indistinguishable from it, if only because of the very small value of J. Thus when a particular 3-mimic is stable, successive points lie on different branches of the 3-mimic UM, but all to the right of the period-3 fixed point. In this way we preserve bistability of the period-3 and 3-mimic BA's. In this way we also determine that the Fraser-Kapral resonance curves are asymmetric, with no peaks to the left of the period-3 unstable periodic point. The increased downward slope of the (B,B) SM as J increases, and the approaching homoclinic tangency causes the asymmetry of the orbit density to gradually build up between $J=0$ and $J^*(3)$.

We do not have a straightforward dynamical explanation of the shortening of regular bursts and the concomitant discrete jump in the Lyapunov exponent of the period-1 BA when $\mu = h'_3(J)$, where "dynamical" means in terms of manifold intersections. We find that all of our numerical results are in accord with the rule that, for a given $J > J^*(3)$, the longest regular burst of period-3 behavior as $\epsilon \to 0$ is approximately determined by the period of the lowest $3n+1$-type 3-mimic saddle node that has crossed $\mu = h'_3(J)$. This will correlate with the extent to which the Lyapunov exponent has decreased toward zero at the transition.

V. INTERMITTENCY OF OTHER PERIODS (n,k)

The scenario we have presented for the changes in intermittency that are related to the onset of the period-3 μ window of stability $[\equiv \Delta\mu_3(J)]$, and occur for $0 \le J \le J'(3)$, has analogs for each saddle-node bifurcation of type (n,k). The analog are qualitatively complete in but few cases, and most of these are not the most important ones, judged by the criterion that $\Delta\mu_{n,k}(J)$ should be large enough that noise in the control parameter is unlikely to interfere with observation of the expected intermittency. Any such criterion is arbitrary. The μ-stability width of the entire trapping region at fixed J is between 2 and 7, $\Delta\mu(3) \simeq 0.04$, and we must remember that intermittency becomes obvious in a μ width of about $0.1\Delta\mu_{n,k}(J)$. We will set a fine limit $\Delta\mu_{n,k}(J) = 0.001$ on observability, which includes surprisingly few (n,k) combinations. In addition, we will discuss intermittency for a few of the 3-mimic orbits because of their relation with period-3 intermittency, even though their μ windows are very small. In general, increasing the period n decreases $\Delta\mu_{n,k}(J)$, as does increasing k, where, for a given n the different k are in the MSS order of increasing values of $s_{n,k}$. For many orbits, $\Delta\mu_{n,k}(J)$ decreases with increasing J, in some cases by a factor 10 or more before one reaches $J'(n,k)$. We have not found any obvious simple scaling of $\Delta\mu_{n,k}(J)$ with n or k.

There are relations between the values of $J^*(n,k)$ and $J'(n,k)$ for different values of (n,k). These appear to follow scaling rules that are generalizations of those worked out for a class of 2D maps by Chen, Gyorgi, and Schmidt [20], and will be discussed elsewhere. Most of these results are only of theoretical importance. In Table IV, we note one such result, relating $J^*(3)$ and $J^*(6,1)$, for which $\Delta\mu_{n,k}(J)$ is fairly large.

Before discussing the numerical results, we mention a change in the symbolic dynamics of (n,k)-mimics from that of 3-mimics, as it affects intermittency. In Sec. III, we pointed out that all truncations of the antiharmonic extension of the period-3 LIP that are not multiples of 3 are LIP's, and so have parameter windows of stability that limit on s_3 from below. Because such orbits, when stable, replace intermittent orbits passing very near to the critical points of the third iterate of the map, their saddle-node parameter values in combination with their periods are good benchmarks of the $\epsilon^{1/2}$ behavior of the Lyapunov exponent. The 3-mimics continue to be important for $J > 0$, as discussed in Sec. IV, and shown in Fig. 11. In generalizing this result to intermittency of the (n,k) orbit, modifications must be made in the symbolic dynamics calculation of (n,k)-mimics. The result is that, whereas all orbits of periods $3n+1$ and $3n+2$ for all positive integers n that are truncations of the antiharmonic extension of period 3 are 3-mimics, in the (n,k) intermittent range of μ only *some* of the orbits of periods $nm+p$, for m any positive integer, and $0 < p < n$, having symbol sequences which are truncations of the antiharmonic extension of the (n,k) LIP, are LIP's; some p's are not allowed. A discussion of this point appears in the Appendix. It is important for obtaining a full understanding of intermittency, but is not practically significant. Enough (n,k) mimics of interest will occur as benchmarks of the intermittent behavior of the Lyapunov exponent for any (n,k) of interest. It would be desirable to know which (n,k) mimics cross $h'_{n,k}$ for $J > J^*(n,k)$,

TABLE IV. Information concerning the changing scenario of intermittency for the Hénon map. We present data including the critical values $J^*(n,k)$, $J'(n,k)$, the saddle-node bifurcation parameter $s_{n,k}(J)$, the periodic window width $\Delta\mu_{n,k}(J)$, and the homoclinic tangency value $h'_{n,k}(J)$ for (a) period 4, (b) period (5,1), (c) period (5,2), (d) period (5,3), (e) period (6,1), (f) period (7,2), and (g) period (8,3).

(a) Period 4

J	$s_4(J)$	$\Delta\mu_4(J)$	$h'_4(J)$
0.0	1.940 551	0.002 211	none
0.01[a]	1.917 597	0.002 261	none
0.02	1.894 610	0.002 313	1.894 759
0.03	1.871 594	0.002 368	1.872 277
0.04	1.848 551	0.002 425	1.850 151
0.046[b]	1.834 714	0.002 46	1.837 05
0.050[d]	1.825 484		(c)

(b) Period (5,1)

J	$s_{5,1}(J)$	$\Delta\mu_{5,1}(J)$
0.0	1.624 397	0.008 97
0.04	1.680 725	0.008 00
0.08	1.738 767	0.007 00
0.10[e]	1.768 260	0.006 67
0.12	1.797 940	0.006 42
0.16	1.857 769	0.006 05
0.20	1.917 836	0.005 79
0.22[f]	1.947 845	0.005 68
0.24[g]	1.977 765	0.005 65

(c) Period (5,2)

J	$s_{5,2}(J)$	$\Delta\mu_{5,2}(J)$
0.0	1.860 587	0.001 75
0.01	1.881 918	0.001 60
0.02	1.903 409	0.001 47
0.03	1.925 073	0.001 36
0.04[h]	1.946 925	0.001 25

(d) Period (5,3)

J	$s_{5,3}(J)$	$\Delta\mu_{5,3}(J)$
0.0	1.985 408	0.000 132
0.01	1.962 812	0.000 133
0.02	1.940 189	0.000 136
0.04[i]	1.894 876	0.000 142
0.06[j,k]	1.849 436	0.000 149

(e) Period (6,1)

J	$s_{6,1}(J)$	$\Delta\mu_{6,1}(J)$
0.0	1.474 700	0.010 90
0.03[l]	1.519 371	0.010 81
0.06	1.564 591	0.010 83
0.10	1.625 746	0.010 92
0.13[m]	1.672 285	0.011 13

(f) Period (7,2)

J	$s_{7,2}(J)$	$\Delta\mu_{7,2}(J)$
0.0[n]	1.673 955	0.001 00
0.1	1.816 579	0.000 52
0.15	1.900 581	0.000 43
0.20[o]	1.991 904	0.000 36

(g) Period (8,3)

J	$s_{8,3}(J)$	$\Delta\mu_{8,3}(J)$
0.0	1.711 037	0.000 389
0.1	1.831 900	0.000 084
0.2	1.973 922	0.000 049
0.25[p]	2.046 867	0.000 04
0.30[q]	2.119 690	0.000 039

[a] $J^*(4)\cong 0.012$.

[b] $J'(4)\cong 0.046\,5$.

[c] Not important for intermittency.

[d] To find the period-4 BA, one needs an internal point, e.g., (0.010 295 7,1.894 360 4).

[e] $J^*(5,1)\simeq 0.10$.

[f] $J'(5,1)\simeq 0.22$

[g] To find the period-(5,1) BA we need an internal point: (1.659 564, −0.799 759).

[h] $J^*(5,2)>0.04$. However, the "surrounding" period-1 BA no longer exists. To find the period-(5,2) BA, one needs an internal point, e.g., (1.890 710, −1.628 004).

[i] $0.02<J^*(5,3)<0.04$.

[j] $0.07<J'(5,3)<0.08$.

[k] The period-(5,3) BA is surrounded by the period-1 BA for all J, because at $J=1.0$ it is created at a resonant bifurcation.

[l] $J^*(6,1)\simeq 0.036$. For reasons that are not clear, this is larger than $(J^*3)^{1/2}\simeq 0.034$, the value to be expected from the scaling theory of Ref. [20].

[m] $J'(6,1)<0.14$. This is also greater than the value of $\simeq 0.135$ predicted in Ref. [20].

[n] Period (7,2) is a truncation of the antiharmonic of period 3.

[o] If $J^*(7,2)$ were defined, it would be greater than 0.2. It is not defined because $s_{7,2}(0.2)>h'_3(0.2)=1.979\,832$, and because metamorphosis has occurred, the period-1 BA is bounded by the period 3 SM for $J>0.081\,6$ and thus is unstable for $\mu>h'_3(0.2)$. A point from which the (7,2) BA can be found at $J=0.2$ is (1.703 221, −0.920 502).

[p] $J^*(8,3)\simeq 0.25$.

[q] $J'(8,3)<0.3$. The period-1 BA is stable because $h'_3(0.3)>s_{8,3}(0.3)$. Nevertheless a point in the period-(8,3) BA is needed to find the BA: (1.716 796, −0.858 613).

in parallel with our results for period 3, but we have not pursued that point here.

More interesting changes of the intermittency scenario may occur because a homoclinic line other than $h'_{n,k}(J)$ interferes with the process. It may destroy the surrounding BA in which the manifold exists which is responsible for $h'_{n,k}(J)$, or, alternatively, interfere with the stability of an (n,k)-mimic, which is less serious. We now present, in Table IV, numerical information concerning intermittency for a number of (n,k) combinations. In each case we give at least $J^*(n,k)$ and $J'(n,k)$. In many cases $s_{n,k}(J), h'_{n,k}(J)$ and $\Delta\mu_{n,k}(J)$ are given for some number of values of J. Comments of interest appear for several cases.

VI. SUMMARY AND CONCLUSIONS

We have discussed in some detail the salient features of the changes in type-I intermittency in the Hénon-map family when its Jacobian parameter J is increased above the value $J=0$ for which intermittency was defined, corresponding to the logistic-map family. For each orbit of period n and type k that originates at a saddle-node bifurcation, the intermittency eventually disappears as J is increased. The disappearance is accompanied by experimental signatures, of which qualitative changes in the invariant-orbit density and the Lyapunov exponent are the most notable. The origins of these changes in the relationships and the structures of invariant manifolds in phase space are fascinating. We showed how Singer's theorem, which mandates one attractor for each parameter value for the 1D quadratic map family, is circumvented in the 2D Hénon case by the removal of homoclinic tangency of certain manifolds as dissipation is decreased. We also noted the other consequences of this removal of homoclinic tangency, and offered heuristic explanations for the consequences of the change in linear damping on the bifurcation structure in (J,μ) parameter space.

The phase-space structure uncovered here while studying type-I intermittency is complex and interesting, and it is all necessary for a full understanding of the numerical results. It is undoubtedly simple compared to the structure associated with phenomena requiring higher-dimensional phase spaces for their explanations. One wonders for how long our mental and computational tools will be equal to the challenge.

As the next, more complicated case, we expect similar changes in intermittency and the geometric structure of phase space to occur for other 2D map families. The most popular such is the dissipative standard map family, which presents the additional complication of mode locking, and other features attendent upon its 1D dissipative limit exhibiting both a maximum and a minimum.

Much of the interest in intermittency stems from its prevalence in extended systems. We hope that the present study can be included as a key element in a study of such a system.

APPENDIX

In Secs. III and IV, we made use of the idea of 3-mimics, defined as periodic orbits whose LIP's are truncations of the infinite symbol sequence called the antiharmonic extension (AHE) of period 3: $RLR^2LR^2\ldots$. At $J=0$, and also for $J<J^*(3)$, these orbits have parameter ranges of stability which precede that of period 3, ever more closely as the length of the truncation increase. Each indicates the occurrence, within period-3 intermittency, of regular period-3 bursts of length equal to its period. For $J>J^*(3)$, we found it necessary to distinguish LIP's of lengths $3m$ and $3m+1, m$ any positive integer (where we use the lengths of LIP's rather than the periods of the periodic orbits as designators). Orbits of the first type have saddle nodes which cross the homoclinic line $\mu=h'_3(J)$ as J increases, in order of *decreasing* period, while those of the second type never experience such crossings. Truncations of the antiharmonic extension of lengths $3m+2$ are not LIP's. We now extend these considerations to truncations of the antiharmonic extensions of the LIP's of other periodic orbits of interest.

Consider truncations of the antiharmonic extension of the period-(n,k) orbit. If the MSS algorithm is complete up to some period greater than or equal to n, and is followed further, the LIP of the next orbit appearing just to the left of (n,k) always consists of a truncation of the (n,k) AHE slightly longer than previously used. By the definition of a LIP, the last point of this LIP is certainly to the right of a point n steps before it in the LIP. But, by the definition of an AHE, each string of n adjacent symbols in it contains an *even* number of R's, and so adding n symbols of the (n,k) AHE to our new LIP creates a second new one to the MSS right of the first new one. Iterating this process creates an infinite chain of such LIP's with periods $nm+p$, where $1\le p<n$, and m is any positive integer. This is a chain of (n,k)-mimics similar to the two chains of 3-mimics discussed earlier. Thus if we test the possibility of (n,k)-mimic *orbits* with lengths

TABLE V. A list of (n,k)-mimics for all orbits showing intermittency through period 7. The entries "p" are the integers modulo n such that orbits of periods $mn+p$, for all integers m, are (n,k)-mimics. AHE, when indefinitely repeated, means antiharmonic extension.

(n,k)	AHE	p
3	RLR	1,2
4	RL^2R	1,2,3
5 1	RLR^3	1,2,4
5 2	RL^2RL	1,2,3
5 3	RL^3R	1,2,3,4
6 1	RLR^3L	2,4*
6 2	RL^2R^3	1,2,3,5
6 3	RL^3RL	1,2,3,4
6 4	RL^4R	1,2,3,4,5
7 1	RLR^5	1,2,3,5
7 2	RLR^2LRL	2,4,5
7 3	RL^2RLR^2	1,2,3,6
7 4	RL^2R^3L	1,2,3,5
7 5	RL^2R^2LR	1,2,3,5,6
7 6	RL^3RL^2	1,2,3,4
7 7	RL^3R^3	1,2,3,4,6
7 8	RL^4RL	1,2,3,4,5
7 9	RL^5R	1,2,3,4,5,6

between $n+1$ and $2n-1$, we will have found all possible (n,k)-mimics. [Remember that there is no length-$2n$ (n,k)-mimic.] Note that if no (n,k)-mimic of a particular length exists, there is no reason to expect the nearest MSS orbit of that period (say p) to the left of the (n,k) intermittent limit to relate to the (n,k) dynamics in a way important for determining the lengths of regular bursts in (n,k) intermittency for μ near orbit p's μ-stability range. In Table V, we list the (n,k)-mimics for periods up to 7.

The underlying reason for the omissions of mimics in Table V is the rapidly increasing number of periodic orbits of period n with increasing n, and the distribution of these among the full MSS sequence. A perusal of the Appendix of the MSS paper, which gives the sequence complete to period 11, is helpful in understanding this point. In all cases of interest, enough (n,k) mimics remain to give form to the regular intermittent bursts. Note that (n,k) orbits with LIP's of the form RL^{n-2}, which includes period 3, have only the one unavoidable excluded sequence. For each n, the LIP noted here is the last one of its period and occurs very near $\mu=2$, thus having an extremely small parameter range of existence at $J=0$.

[1] Y. Pomeau and P. Manneville, Commun. Math. Phys. **74**, 189 (1980).
[2] H. Kaplan, Phys. Rev. Lett. **68**, 553 (1992).
[3] H. J. Schuster, *Deterministic Chaos,* 2nd ed. (VCH Verlagsgesellschaft, Weinheim, 1989), pp. 17–19.
[4] M. Misiurewicz, Publ. Math. I.H.E.S. **53**, 17 (1981).
[5] M. Hénon, Q. Appl. Math. **XXVII**, 291 (1969).
[6] P. J. Holmes and D. C. Whitley, Philos. Trans. R. Soc. London, Ser. A **311**, 43 (1984).
[7] H. El Hamouli and C. Mira, C. R. Acad. Sci. Paris, Series I **293**, 525 (1981).
[8] S. Fraser and R. Kapral, Phys. Rev. A **23**, 3303 (1981).
[9] I would like to thank Professor J. Hubbard for pointing out this effect.
[10] T. J. Price and T. Mullin, Physica D **48**, 29 (1991).
[11] N. Metropolis, M. L. Stein, and P. R. Stein, J. Combinatorial Theory **15**, 25 (1973).
[12] H. Kaplan, Physics Lett. **97A**, 365 (1983).
[13] S. M. Hammel, and C. K. R. T. Jones, Physica D **35**, 87 (1989).
[14] C. Grebogi, E. Ott, and J. A. Yorke, Phys. Rev. Lett. **56**, 1011 (1986); Physica **24D**, 243 (1987).
[15] H. Poincaré, *Les Methods Nouvelles de la Mechanique Celeste* (Gauthier-Villars, Paris, 1892).
[16] C. Grebogi, E. Ott, and J. A. Yorke, Phys. Rev. Lett. **50**, 935 (1983).
[17] O. Biham and W. Wenzel, Phys. Rev. Lett. **63**, 819 (1989).
[18] R. Devaney and Z. Nitecki, Commun. Math. Phys. **67**, 137 (1979).
[19] D. L. Hitzl, Physica **2D**, 370 (1981).
[20] C. Chen, G. Györgi, and G. Schmidt, Phys. Rev. A **35**, 2660 (1987).